

# Electromagnetic Field Analysis of Septum Magnet for APS Positron Accumulator Ring

Toshiaki Yokoi and Larry R. Turner  
Accelerator Physics Group  
Advanced Photon Source

## Abstract

This report consists of three parts. The first part describes a numerical analysis method for the electromagnetic field analysis of a septum magnet. A novel improvement to the treatment of exciting currents in the time-domain is proposed. The second part discusses numerical predictions of the electromagnetic characteristics of the APS PAR septum. The time variations of stray field and eddy currents are shown for three magnet designs. The last part explores how decreasing the septum material conductivity affects the stray field. The decrease of conductivity may be caused by an inadequate manufacturing of the septum material. The significance of a high quality septum, or flat interface between copper and iron, is emphasized from a point of view of stray field. An ideal method for joining two different metals without distortion, called HIP (Hot Isostatic Pressing), is introduced and recommended based on the authors' experience<sup>1</sup>.

## 1 Numerical Model for APS Positron Accumulator Ring Septum Magnet

Figure 1 shows the configuration of a Positron Accumulator Ring (PAR) septum magnet. This system has a primary exciting coil and a set of septum conductors (the transformer secondary) for the reduction of stray field (Figure 2). Since this system involves both transient eddy currents and magnetic nonlinearity, an accurate numerical analysis method must be employed for the analysis.

In this report we employ an ordinary two-dimensional finite element method and a new one improved by the authors.

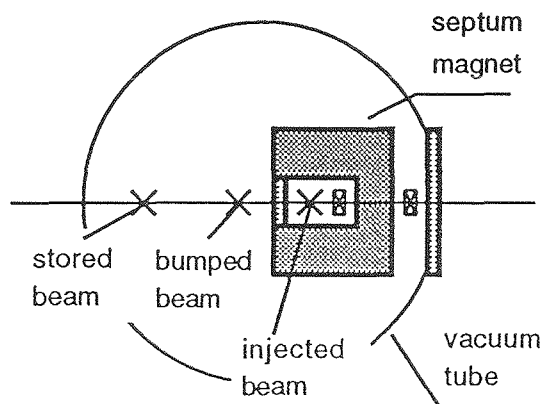


Figure 1. Configuration of APS PAR Septum Magnet

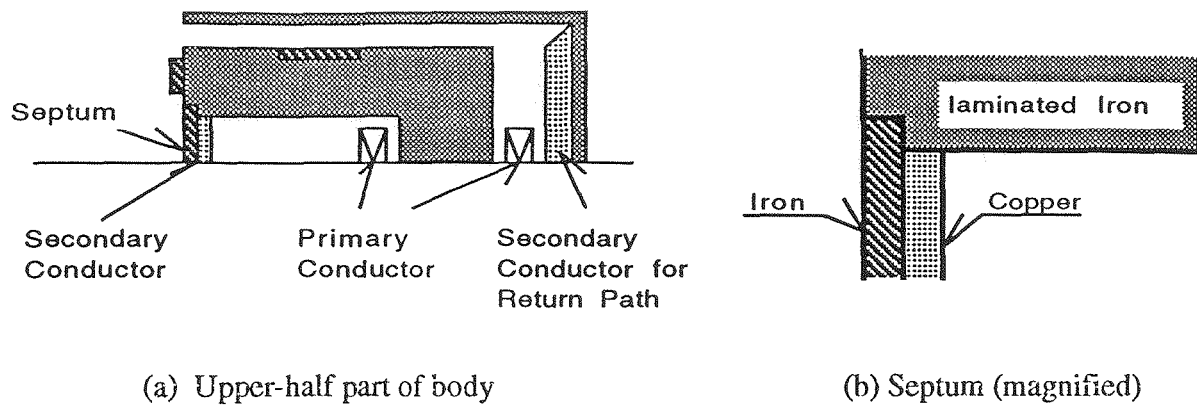


Figure 2. Sectional View of Septum Magnet

### 1.1 Numerical Analysis Method for Transient Electromagnetic Field

The Finite Element Method (FEM) is employed in this study. The necessary considerations in the analysis of septum magnet are listed below.

- Eddy currents in conductors
- Nonlinear characteristics of magnetic substance
- Single/plural electric circuits of septum current
- Precise evaluation of exciting current

Most of the past numerical analyses on septums have been carried out by using commercial numerical analysis software, such as Opera-2D from Vector Field Ltd. Although they provide fairly good pre- and post-processing environments and reliable solutions for most of the problems of concern, they have some deficiencies at this time. For example, Opera-2D cannot consider a single electric circuit over different materials, etc.

Hence, we decided to developed a similar, but new analysis program which enables us to:

- Consider arbitrary electric circuits over different materials (Appendix A)
- Precisely evaluate exciting current by use of Galerkin's method for time-domain (Appendix B)
- Write data to files in "Mathematica®"† format.

†Mathematica® is a registered trademark of Wolfram Research.

### 1.2 Models for Electric Circuit Evaluation

For the investigation of the effect of electric circuit connectivity to stray field, we choose the following three models.

- (1) Model 1 (two electric circuits model) - Figure 3
  - Each conductive material, copper and iron, is an independent electric circuit.
- (2) Model 2 (single electric circuit model) - Figure 4
  - All conductive parts are connected to one another at the end of the magnet.
- (3) Model 3 (single electric circuit model without iron plate) - Figure 5
  - Left and upper iron plates in Figure 2-(a) are removed in order to evaluate their effect on the stray field.

In every model, the thickness of each copper part and iron part of the septum is 1mm.

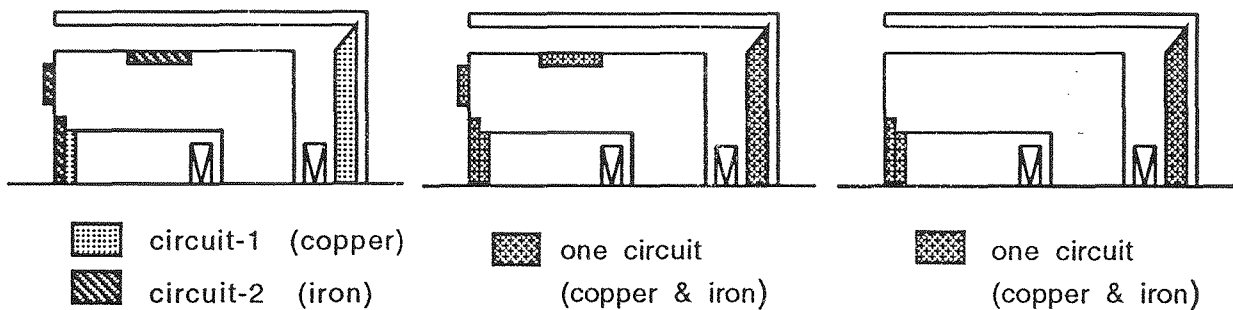


Figure 3. Model 1  
(2-circuit)

Figure 4. Model 2  
(1-circuit)

Figure 5. Model 3  
(1-circuit)

(These figures are not to scale.)

### 1.3 Effect of Septum Conductivity to Stray Field

When we adopt the explosion bonding method in manufacturing a septum, the boundary between copper and iron becomes very wavy. It is obvious that such a boundary causes the following phenomena:

- Decrease in conductivity by narrowing current path of the copper part
- Increase in saturation at thin iron part

As will be shown, since these two phenomena cause a significant increase in stray field, it is important to make septums of high quality. An alternative method of bonding different materials, HIP (Hot Isostatic Method), is considered the best method for manufacturing high quality septums. A detailed introduction of HIP is given in Appendix C.

## 2 Results of Calculations

### 2.1 Exciting Current Condition (1/2 magnet split at the midplane)

Shape:	unipolar half-sinusoidal wave pulse (Figure 6)
Pulse width:	0.333 [ms]
Pulse per second:	2 [pulses/s]
Peak value:	5960.07 [A] (1/2 of the primary)
Peak current density:	83,650,096 [A/m <sup>2</sup> ]

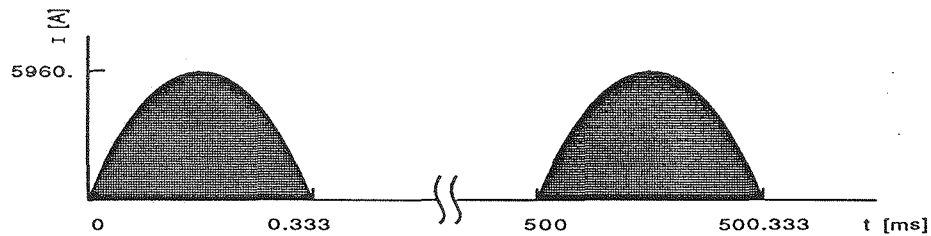
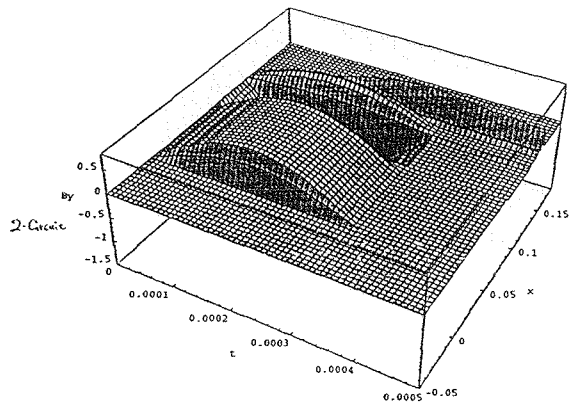


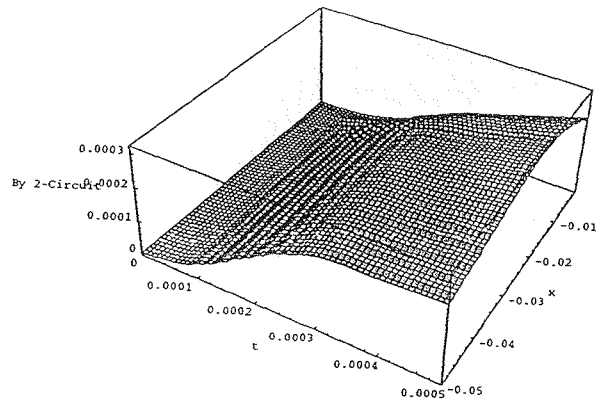
Figure 6. Exciting Current

### 2.2 Results for the Electrical Circuit Evaluation Model

Figures 7-9 show the difference in the time variation of the magnetic flux density at the center of the magnet for the three different models. Figure 7 indicates that if we can isolate the copper and iron septums electrically, the stray field at the outside of the septum becomes very low. However, it is very difficult to isolate the copper and iron parts electrically. Figure 8 shows the high stray field caused primarily by the currents in the iron plates attached to the left and top of the septum magnet. It is expected that a significant reduction in stray field can be achieved by removing these plates (Figure 9).

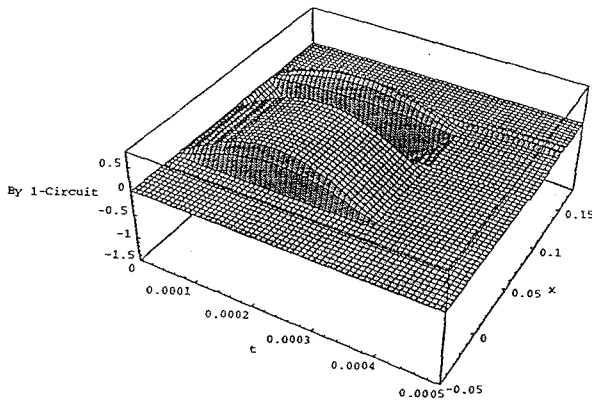


(a) Whole Region of Analysis

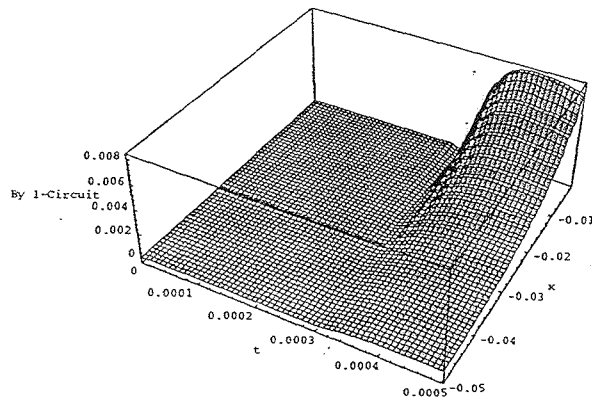


(b) Outside of Septum (Magnified)

Figure 7. Time Variation of Magnetic Flux Density at the Center of the Magnet  
(Model 1, 2-circuit)

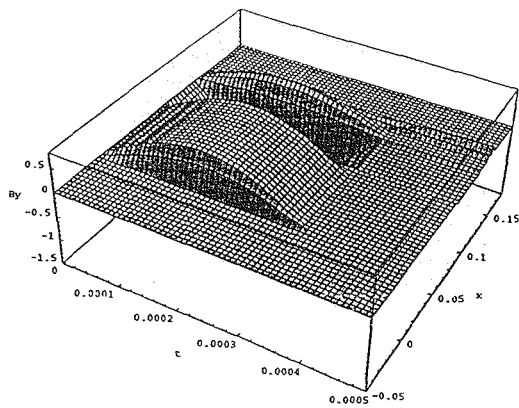


(a) Whole Region of Analysis

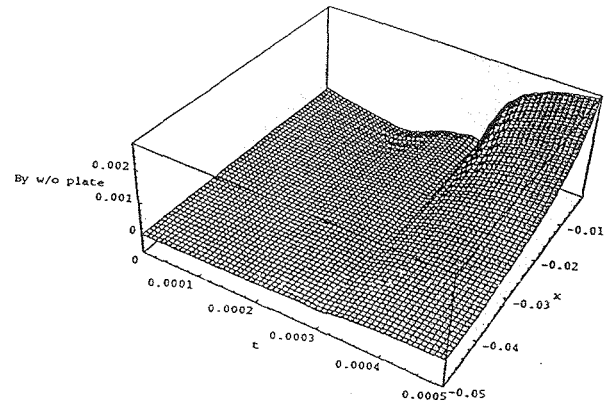


(b) Outside of Septum (Magnified)

Figure 8. Time Variation of Magnetic Flux Density at the Center of the Magnet  
(Model 2, 1-circuit)



(a) Whole Region of Analysis



(b) Outside of Septum (Magnified)

Figure 9. Time Variation of Magnetic Flux Density at the Center of the Magnet (Model 3, 1-circuit)

Figures 10-12 show the currents in the septum for Model 3. Time variation of the total current of the septum is close to that of the primary excitation current (Figure 10). However, Figures 11 and 12 show that there is a local current loop between the copper and iron septums after the end of primary excitation.

In order to see what is happening in the secondary currents, variations of currents in the secondary circuit region (Figure 13) are shown in Figures 14-17. According to those figures, it is expected that there are some local current loops even during the primary excitation period.

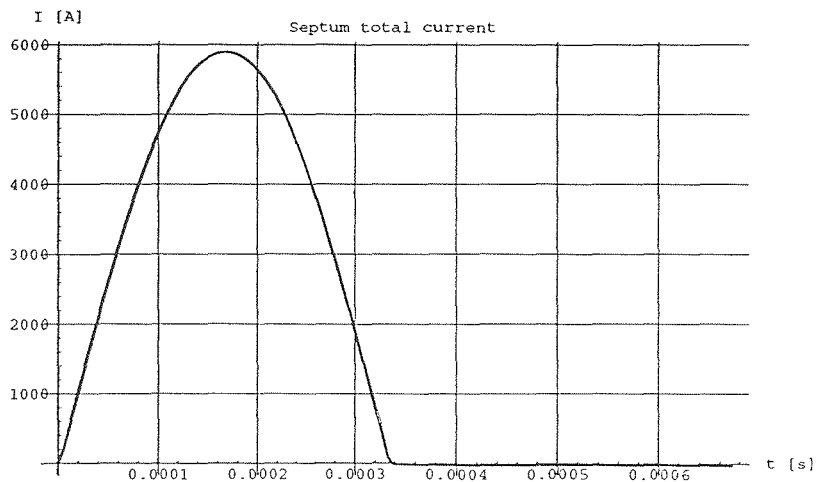


Figure 10. Septum Total Current (Model 3)

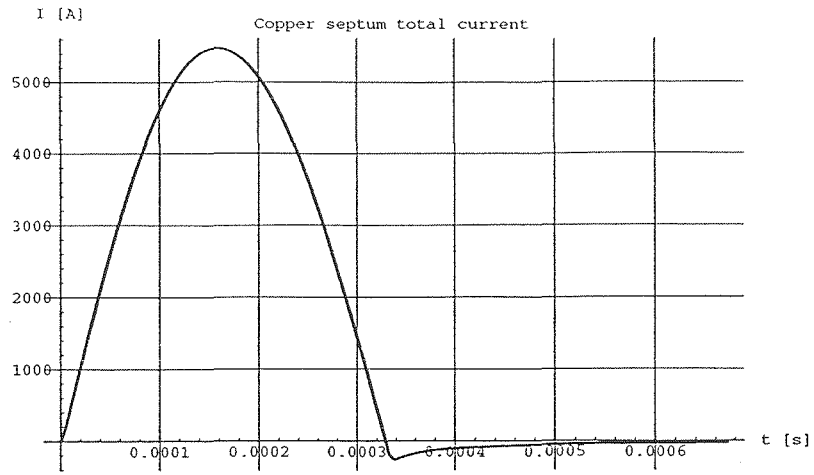


Figure 11. Current in Copper Part of Septum (Model 3)

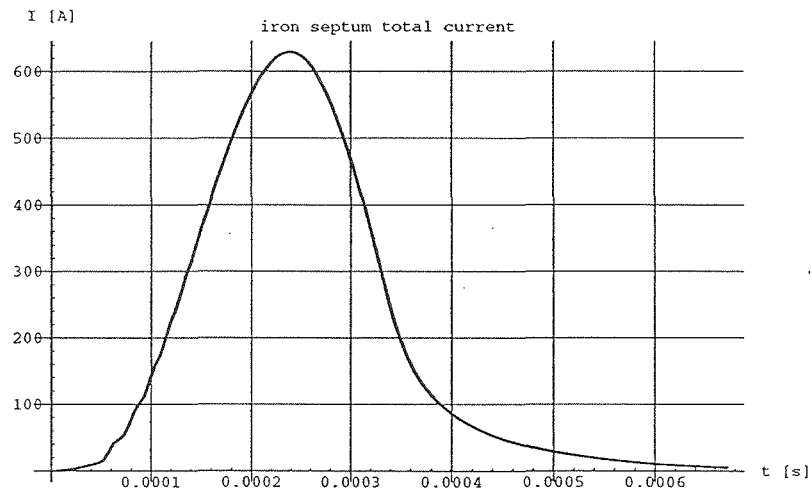


Figure 12. Current in Iron Part of Septum (Model 3)

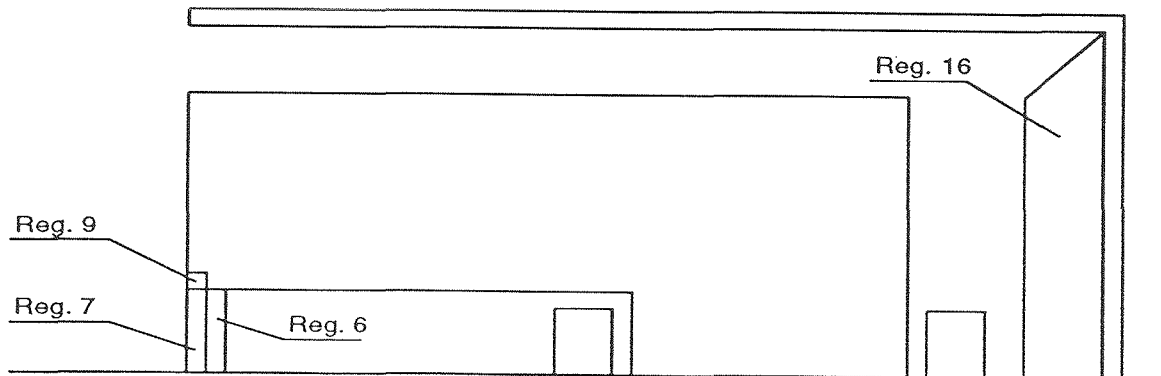


Figure 13. Region Numbers in Model 3 (not to scale)

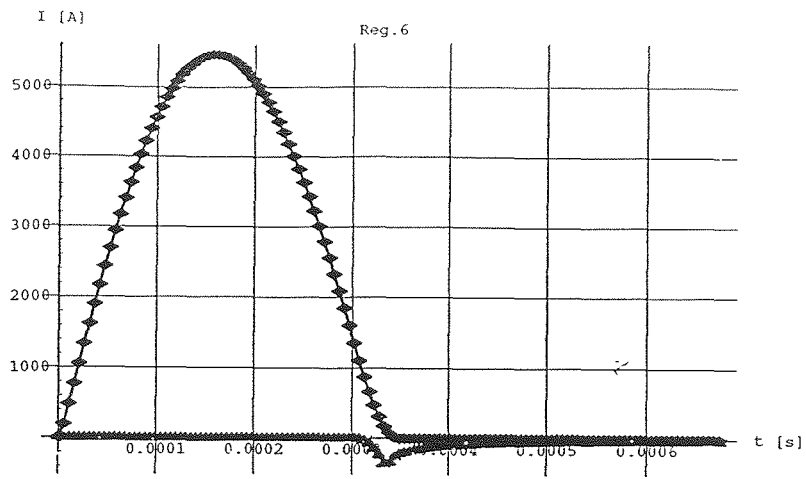


Figure 14. Currents in Region 6 (copper part of septum, positive and negative components) (Model 3)

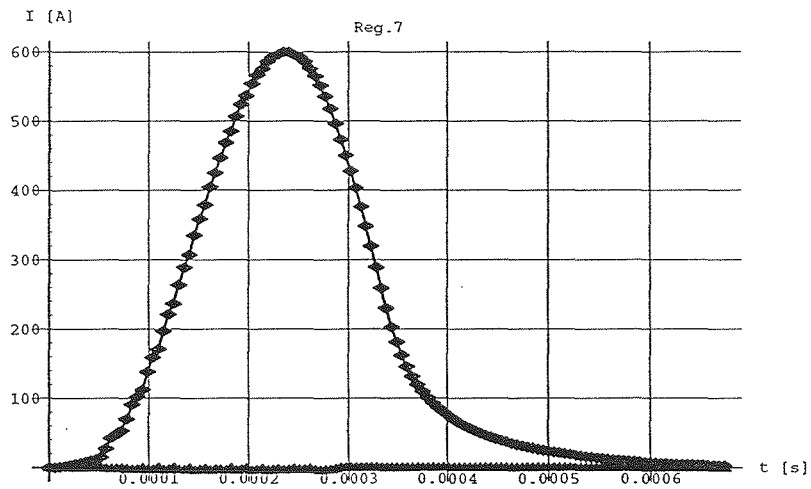


Figure 15. Currents in Region 7 (lower iron part of septum, positive and negative components) (Model 3)

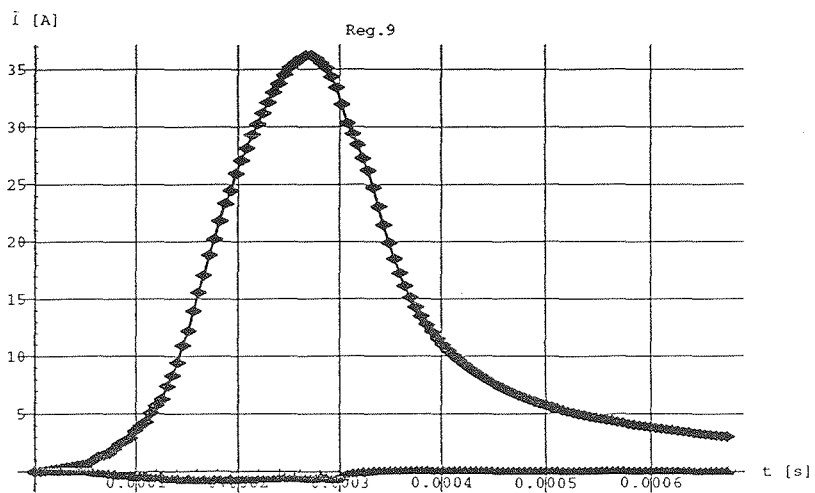


Figure 16. Currents in Region 9 (upper iron part of septum, positive and negative components) (Model 3)

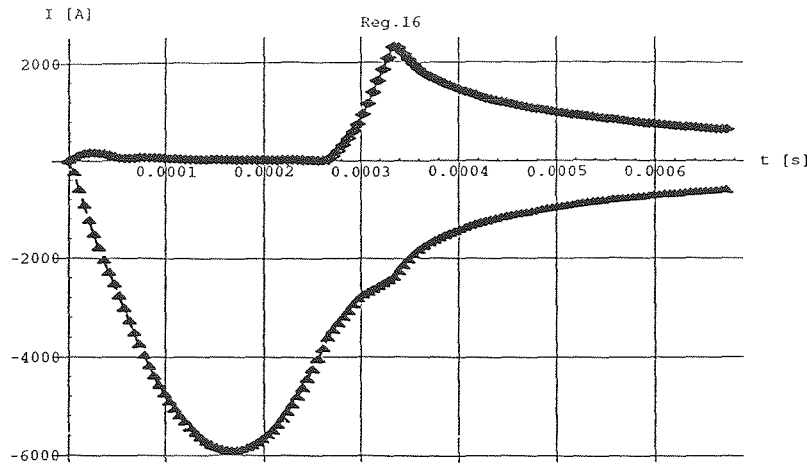


Figure 17. Currents in Region 16 (return path of septum currents, positive and negative components) (Model 3)

### 2.3 Results of the Effect of Septum Conductivity to Stray Field

This section discusses the effect of decrease in conductivity which can be caused when manufacturing the septum by explosion binding. Even if the average thickness of each component is the same to 1mm, undulation of the boundary between the copper and iron parts of the septum decreases the total conductivity in the longitudinal direction significantly. Furthermore, such undulation creates thin parts in the iron septum prone to magnetic saturation and consequently less effective in magnetic shielding.

Figures 18-22 show the time variation of magnetic flux density for the full conductivity case and decreased conductivity cases. It is obvious that a decrease in the conductivity of the septum causes a significant increase in stray field and qualitative differences in time variation.

Figure 23 summarizes the relationship between the conductivity ratio compared to its nominal value and the resulting stray field peak value. We have to recognize that these values are less than expected since these calculations did not consider the effect of the thin iron septum part. Even so, Figure 23 is enough to show how important the septum quality is.

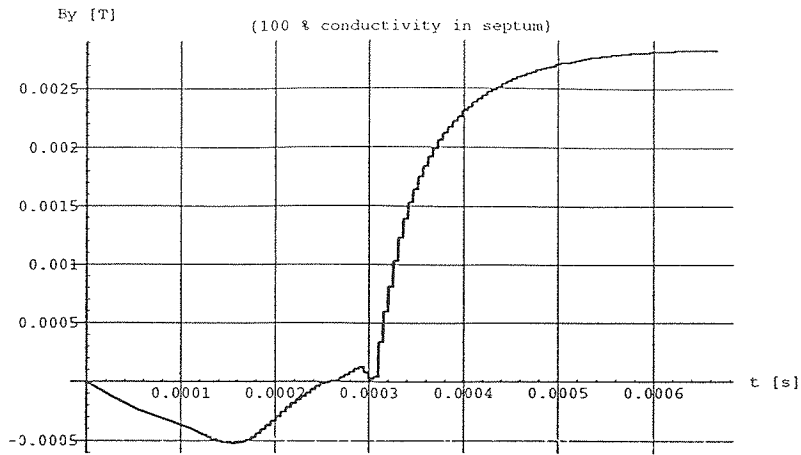


Figure 18. Time Variation of Magnetic Flux Density (100% conductivity in septum, Model 3) (at a distance of 0.1[mm] from iron septum surface)

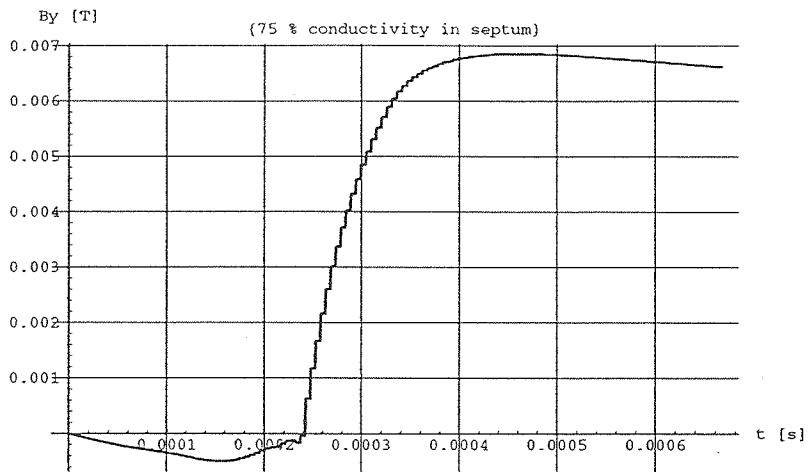


Figure 19. Time Variation of Magnetic Flux Density (75% conductivity in septum, Model 3) (at a distance of 0.1[mm] from iron septum surface)

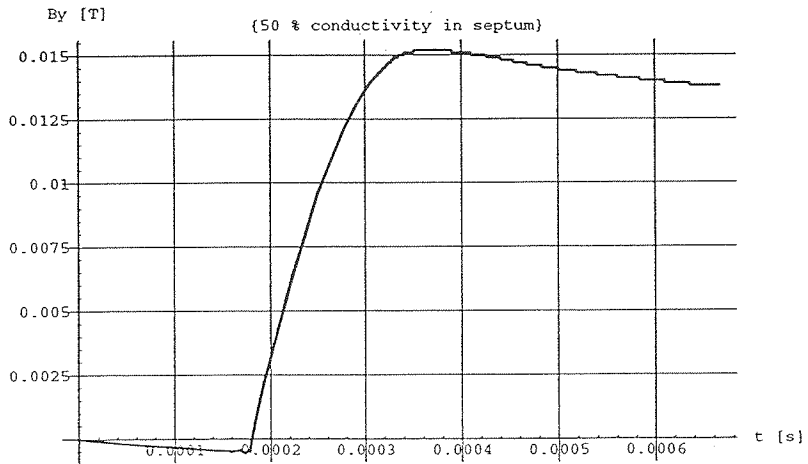


Figure 20. Time Variation of Magnetic Flux Density (50% conductivity in septum, Model 3) (at a distance of 0.1[mm] from iron septum surface)

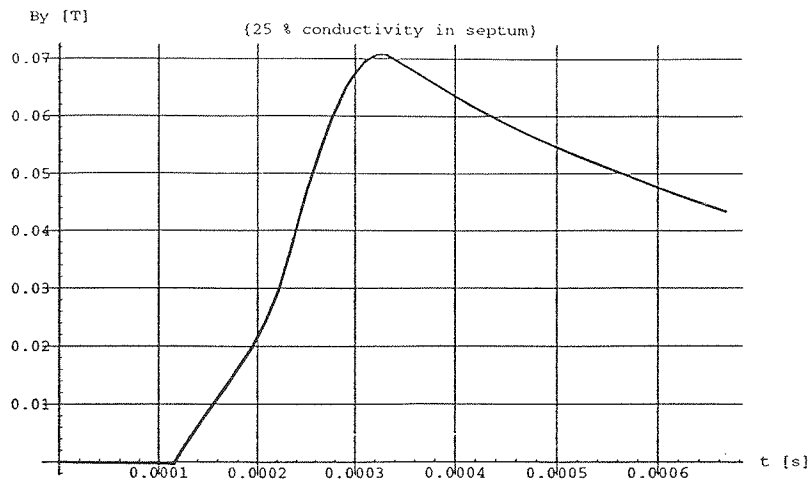


Figure 21. Time Variation of Magnetic Flux Density (25% conductivity in septum, Model 3)  
(at a distance of 0.1[mm] from iron septum surface)

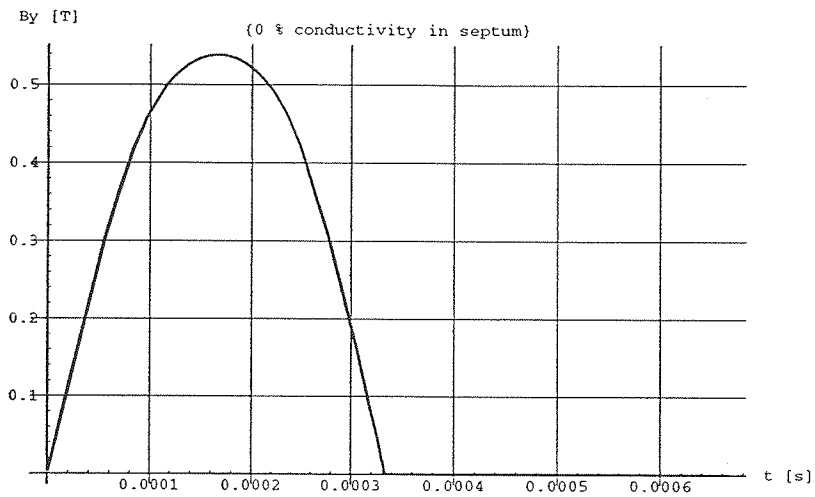


Figure 22. Time Variation of Magnetic Flux Density (0% conductivity in septum; Model 3)  
(at a distance of 0.1[mm] from iron septum surface)

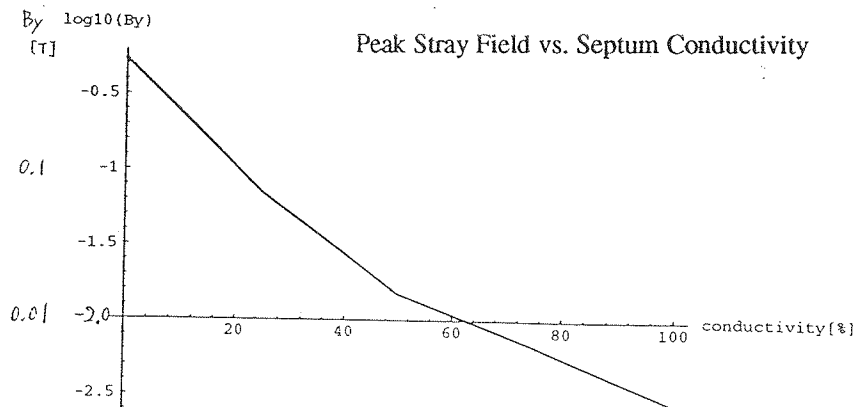


Figure 23. Stray Field Peak Value vs. Conductivity Percentage (Model 3)

### 3. Conclusion

In this report we investigated the relationship between septum quality and stray field. If we use explosion bonding in the septum manufacturing process, the boundary between copper and iron becomes wavy. According to the results of calculations on conductivity variations in the septum, such wavy septums cause an increase in stray field. Furthermore, since wavy boundaries create many thin parts in the iron septum, saturation in the iron septum also increases which results in an increase in stray field.

Although some additional revisions might improve the large stray field, we believe that the most efficient improvement is to make high quality septums by using HIP or similar techniques.

### Reference

- 1) T. Yokoi, D. Ebihara, et al., "Investigation report on linear motor technology for TOKYO L-NET subway transportation vehicle," Institute for Posts and Telecommunications Policy, Ministry of Posts and Telecommunications of Japan, March 1993.

## Appendix A: "Consideration of arbitrary number of electrical circuit"

A closed electric circuit has same-valued, opposite-signed currents. In other words, integration of independent electric circuit currents over each belonging region has to be zero. In two-dimensional analysis, the field variable  $-\nabla\phi$  is introduced in order to impose this condition. In the case of a single circuit, we have to define one  $-\nabla\phi$ . In the plural circuits case, we must use plural  $-\nabla\phi$  for each independent circuit. In this two-dimensional analysis we need only the z-component of  $-\nabla\phi$ , namely  $\frac{\partial\phi}{\partial z}$ .

A closed electric circuit condition is given by (A-1). Finally, we derive (A-2).

$$\int_{S_i} J_z ds = 0 \quad |_{i=1, \text{ number of independent circuits}} \quad (\text{A-1})$$

$$\int_{S_i} \left( -\sigma \left( \frac{\partial A_z}{\partial t} + \frac{\partial \phi_i}{\partial z} \right) \right) ds = 0 \quad |_{i=1, \text{ number of independent circuits}} \quad (\text{A-2})$$

where,  $S_i$  denotes the region which belongs to the i-th circuit.

## Appendix B: "Galerkin's method and $\theta$ method in time-domain"

(1) Governing equations of a problem

$$[H] \{A\} + [C] \frac{\partial \{A\}}{\partial t} + \{g(t)\} = \{0\} \quad (\text{B-1})$$

$$\{A\} = [N_0(t) \ N_1(t)] \begin{Bmatrix} \{A_0\} \\ \{A_1\} \end{Bmatrix} \quad (\text{B-2})$$

$$\frac{\partial \{A\}}{\partial t} = \frac{1}{\Delta t} [-1 \ 1] \begin{Bmatrix} \{A_0\} \\ \{A_1\} \end{Bmatrix} \quad (\text{B-3})$$

where,  $\{A\}$ : set of vector potential.

$\{A_0\}, \{A_1\}$ : set of vector potential at  $t=t_0$  and  $t=t_1$ , respectively.

$\{g(t)\}$ : external force.

$[H], [C]$ : coefficient matrix derived from Galerkin's method in Finite Element Method<sup>1</sup>.

$N_0(t), N_1(t)$ : trial functions for linear variation approximation of vector potential

(Figure B-1).

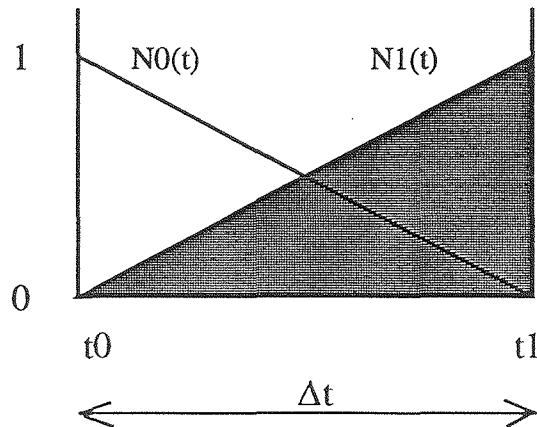


Figure B-1. Trial Functions for Linear Variation Approximation of Vector Potential

(2)  $\theta$  method

In the  $\theta$  method, we firstly define time  $t_m$ , which denotes the evaluating time of differential of vector potential by time.

$$t_m \triangleq t_0 + \theta \Delta t \quad (0 < \theta \leq 1) \quad (\text{B-4})$$

By selecting the  $\theta$  value, we can change the type of differentiation.

$\theta=1$ : Backward differentiation.

$\theta=2/3$ : Same as Galerkin's method except external force evaluation.

$\theta=0.5$ : Central differentiation.

Using  $\theta$ , we derive the following expressions.

$$\frac{\partial A_m}{\partial t} = \frac{A_m - A_0}{\theta \Delta t}, \quad A_1 = A_0 + (A_m - A_0)/\theta \quad (\text{B-5,6})$$

$$[H]\{A_m\} + [C] \frac{\partial \{A_m\}}{\partial t} + \{g(t_m)\} = 0 \quad (\text{B-7})$$

$$\left( [H] + \frac{1}{\theta \Delta t} [C] \right) \{A_m\} = \frac{1}{\theta \Delta t} [C] \{A_0\} - \{g(t_m)\} \quad (\text{B-8})$$

$$\text{Here, } A_m = \theta A_1 + (1 - \theta) A_0. \quad (\text{B-9})$$

Finally, we derive following set of equations.

$$\left( \theta [H] + \frac{1}{\Delta t} [C] \right) \{A_1\} = \left( (\theta - 1) [H] + \frac{1}{\Delta t} [C] \right) \{A_0\} - \{g(t_m)\} \quad (\text{B-10})$$

(3) Galerkin's method in time-domain

Applying Galerkin's method to the time differential matrix equation, we derive following residual equation.

$$\begin{aligned} R &= \int_{t_0}^{t_0 + \Delta t} N_1(t) \left( [H][N_0(t) \quad N_1(t)] \begin{Bmatrix} \{A_0\} \\ \{A_1\} \end{Bmatrix} + [C] \left[ \frac{\partial N_0(t)}{\partial t} \quad \frac{\partial N_1(t)}{\partial t} \right] \begin{Bmatrix} \{A_0\} \\ \{A_1\} \end{Bmatrix} \right) dt + \int_{t_0}^{t_0 + \Delta t} N_1(t) \{g(t)\} dt \\ &= \left( [H] \begin{bmatrix} \Delta t & \Delta t \\ 6 & 3 \end{bmatrix} + [C] \begin{bmatrix} -\frac{1}{2} & 1 \\ 2 & 2 \end{bmatrix} \right) \begin{Bmatrix} \{A_0\} \\ \{A_1\} \end{Bmatrix} + \int_{t_0}^{t_0 + \Delta t} N_1(t) \{g(t)\} dt \end{aligned} \quad (\text{B-11})$$

Now we can find a solution which makes the residuals equal to 0.

$$\left( [H] \begin{bmatrix} 1 & 2 \\ 3 & 3 \end{bmatrix} + \frac{1}{\Delta t} [C] \begin{bmatrix} -1 & 1 \end{bmatrix} \right) \begin{Bmatrix} \{A_0\} \\ \{A_1\} \end{Bmatrix} + \frac{2}{\Delta t} \int_{t_0}^{t_0+\Delta t} N_1(t) \{g(t)\} dt = 0 \quad (B-12)$$

$$\therefore \left( \frac{2}{3} [H] + \frac{1}{\Delta t} [C] \right) \{A_1\} = \left( -\frac{1}{3} [H] + \frac{1}{\Delta t} [C] \right) \{A_0\} - \frac{2}{\Delta t} \int_{t_0}^{t_0+\Delta t} N_1(t) \{g(t)\} dt \quad (B-13)$$

#### (4) Comparison of Galerkin's method and $\theta$ method

If we choose  $\theta=2/3$ , all of the coefficients for  $\{A_0\}$ ,  $\{A_1\}$  become the same. However, external force terms still have different forms as shown in (B-14) and (B-15).

$$\theta \text{ method:} \quad -\{g(t_m)\} \quad (B-14)$$

$$\text{Galerkin's method:} \quad -\frac{2}{\Delta t} \int_{t_0}^{t_0+\Delta t} N_1(t) \{g(t)\} dt \quad (B-15)$$

Figure B-2 illustrates the relationship between those external force evaluations. Since the  $\theta$  method adopts  $g(t_m)$  as an average external value during the discrete period, when  $g(t)$  is increasing to time, the  $\theta$  method always overestimates the external force. Similarly, it underestimates the external force when the force is decreasing to time. These phenomena occur in evaluating the septum driving current.

On the other hand, "Galerkin's method in time-domain" can evaluate external force more precisely than the  $\theta$  method since it considers variations of the function  $g(t)$  during the time-step.

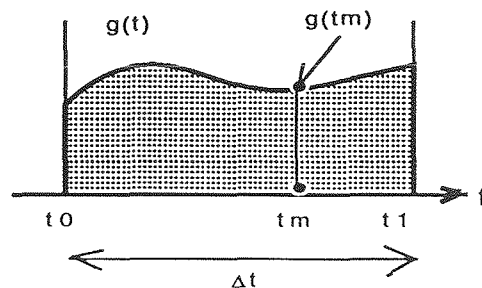


Figure B-2. External Force Function and Evaluation

#### Reference

- 1) K. J. Binns, P. J. Lawrenson and C. W. Trowbridge, "The Analytical and Numerical Solution of Electric and Magnetic Fields," John Wiley & Sons, 1992.

## Appendix C: "HIP Method for Combining Two Metals with Diffusion"

HIP (Hot Isostatic Pressing) is one of the most ideal methods for combining two different metals without glue. Since the combination is based on diffusion of elements, it is stable even under radiation. Furthermore, HIP prevents the processed materials from distortion and any change in electrical and magnetic characteristics. Thus, HIP is considered as the most adequate process for making a septum made of copper and iron.

The following description is for a typical HIP system manufactured by Kobe Steel Co. Ltd. This system was practically used in manufacturing ladder type secondary reaction plates for a particular linear induction motor system<sup>1</sup>.

### 1. Process condition

- (1) Temperature: 900-950 [°C] (1652-1742 [°F])
- (2) Pressure: 98 [M Pa] (968.6 times of atmosphere pressure)
- (3) Gas: Argon
- (4) Combination type: diffusion

### 2. Applications

- (1) Elimination of bubble in an article of cast metal
- (2) Press and bake of powder material
- (3) Making of a composite material

### 3. Merits

- (1) No distortion
- (2) Hardness is kept almost constant even around a boundary
- (3) Strong combining at atomic level

Figure C-1 illustrates the configuration of the HIP system. The workpiece is shown in the center of the figure. Figure C-2 is a picture of the materials used in the HIP process. A metal capsule for HIP processing of a test block is shown in Figure C-3.

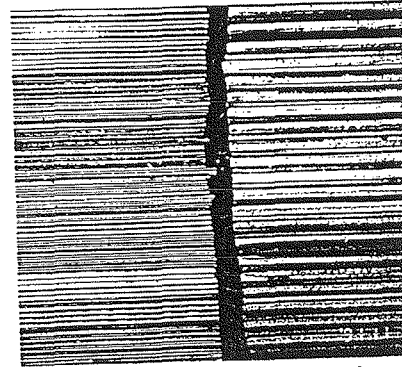
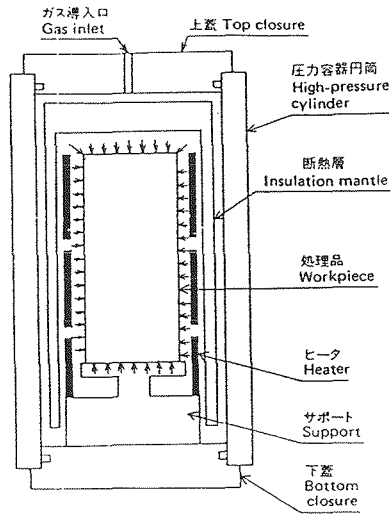


Figure C-1. Configuration of the HIP System

Figure C-2. Metal Sheets of Copper and Iron (before processing)

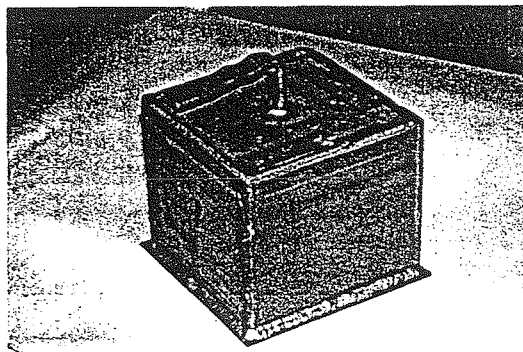


Figure C-3. Capsule for HIP Processing of Test Block

As shown in Figures C-4 through C-6, the HIP process does not create undulation on the boundary between the copper and iron even at a microscopic level.

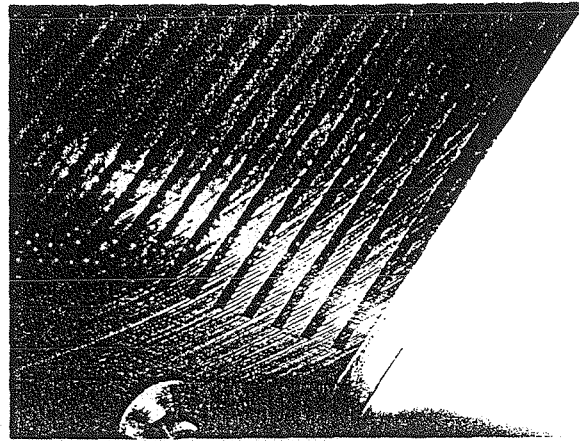


Figure C-4. Magnified View of Copper and Iron Lamination after HIP  
(thickness: copper-part 0.8[mm], iron-part 0.5[mm])

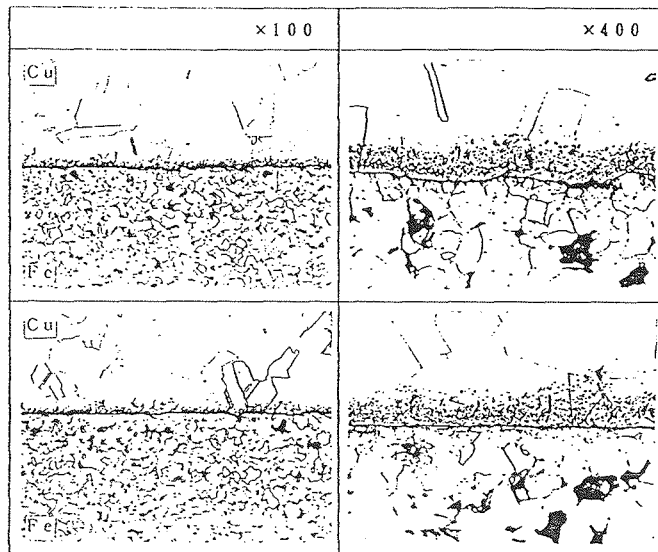
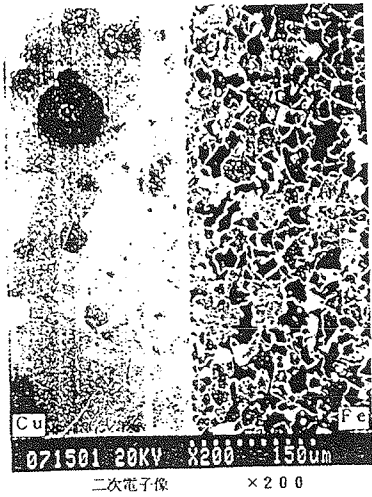
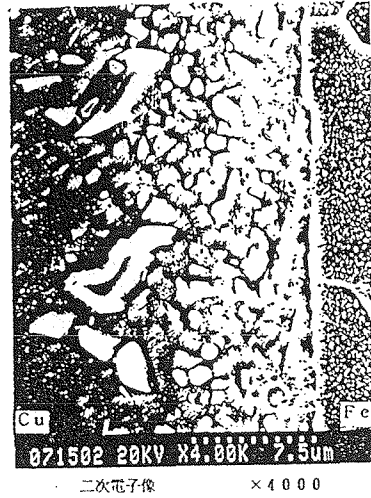


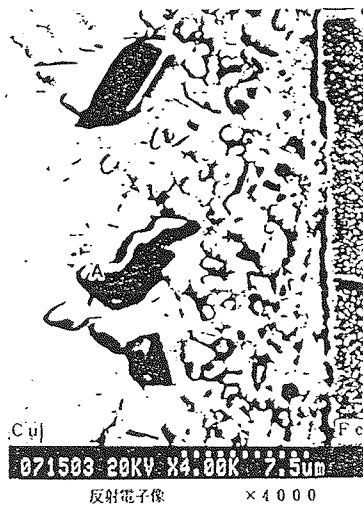
Figure C-5. Photomicrograph of Copper/Iron Boundary (optical)



(a) Secondary Electron Image (× 200)



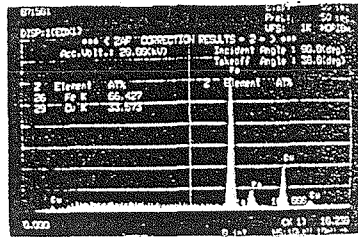
(b) Secondary Electron Image (× 400)



(c) Secondary Electron Image (× 4000)

Figure C-6. Photomicrograph of Copper/Iron Boundary

Figure C-7 shows the result of quantity analysis of point A in Figure C-6-(c) by x-ray micro analysis. It indicates the bunch at point A is made of  $\text{Fe}_2\text{Cu}$ .



Λ点の定量分析結果



Fe, Cuと推定出来る

Figure C-7. Quantity Analysis of Point A in Figure C-6-(c) by X-ray Micro Analyzer

According to Figure C-8, the diffusion layer between the copper and iron has a thickness of 18 $\mu$ m. This thickness is considered thin enough for septum application.

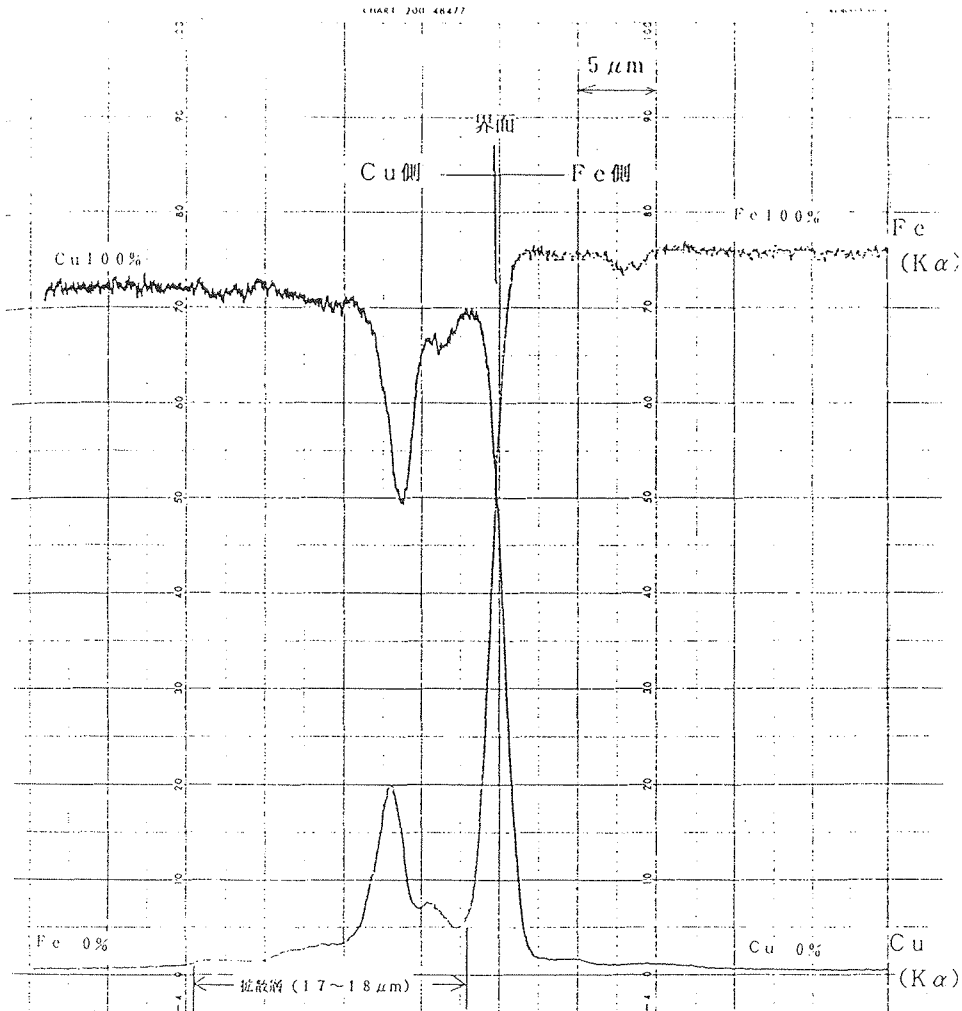


Figure C-8. Element Density Distribution around Copper/Iron Boundary

## Reference

- 1) T. Yokoi, D. Ebihara, et al., "Investigation report on linear motor technology for TOKYO L-NET subway transportation vehicle," Institute for Posts and Telecommunications Policy, Ministry of Posts and Telecommunications of Japan, March 1993.